Carbohydrate Polymers 92 (2013) 2327–2336

Contents lists available at SciVerse ScienceDirect

Carbohydrate Polymers

journal homepage: www.elsevier.com/locate/carbpol

Changes in the physical properties of xanthan gum induced by a dynamic high-pressure treatment

Sandra I. Laneuville, Sylvie L. Turgeon*, Paul Paquin

Dairy Research Center STELA, Faculty of Agriculture and Food Science, Laval University, Pavilion Paul – Comtois, Quebec, Canada G1V-0A6

ARTICLE INFO

Article history:
Received 13 June 2012
Received in revised form
20 November 2012
Accepted 26 November 2012
Available online 3 December 2012

Keywords:
Xanthan
Polysaccharide
Flow birefringence
Molecular aggregates
Mechanical degradation
Rheology

ABSTRACT

The effect of microfluidization, a dynamic high pressure treatment, on xanthan gum was investigated in views of enlarging its potential applications. Samples were characterized chemically and physically (molecular weight, intrinsic viscosity, flow behavior and flow induced birefringence). Particular interest was given to the correlation between the level of degradation and aggregate content to the flow behavior and flow-induced birefringence. A mechanism of degradation is proposed: initially, microfluidization reduces the aggregated state of xanthan and may even be able to dissociate the double helical structure into single chains; upon increasing treatment severity, a relatively mild degradation of the main chain can be achieved. Interestingly, samples treated at high ionic strengths were more sensitive to mechanical degradation, arguably since stiffer molecules in the ordered conformation presented a larger exposed surface and thus experienced stronger effective stresses when subjected to the high shear and cavitation forces present in the microfluidization chamber.

1. Introduction

Xanthan gum, the extracellular polysaccharide produced by aerobic fermentation of the bacterium *Xanthomonas campestris*, has been largely studied and its primary structure is well established (Jansson, Kenne, & Lindberg, 1975; Sworn, 2009). In aqueous solution, xanthan adopts an ordered helical conformation, single or double stranded, depending on ionic strength, temperature (T°), solvent, and thermal treatment history of the sample (Born, Langendorff, & Boulenguer, 2005; Milas, Reed, & Printz, 1996; Muller, Aurhourrache, Lecourtier, & Chauveteau, 1986; Sato, Norisuye, & Fujita, 1984). At high ionic strengths, the side chains align along the backbone to form a stiff structure (persistence length $q = 120 \pm 20$ nm) (Muller & Lecourtier, 1988; Sato et al., 1984), which is stabilized principally by hydrogen bonding and non-ionic interactions outweighing the repulsion between adjacent COO^- groups (Born et al., 2005; Holzwarth, 1976; Lo, Ziegler, Argin-Soysal, Hsu, & Wagner, 2009; Sworn, 2009).

The ordered conformation can undergo an order–disorder transition to yield a disordered flexible coil by decreasing salinity, i.e., by maximizing electrostatic repulsive forces between ionized carboxylate groups (Norton, Goodall, Frangou, Morris, & Rees, 1984), or by increasing the temperature above a characteristic melting temperature T_m (Holzwarth, 1976; Matsuda, Biyajima, & Sato, 2009; Muller & Lecourtier, 1988; Norton et al., 1984; Pelletier, Viebke, Meadows, & Williams, 2001). Several authors have suggested that the denaturation process of the double helical conformation is a two-step process and follows an extension-dissociation path (Liu & Norisuye, 1988; Muller & Lecourtier, 1988; Stokke, Smidsrød, & Elgsaeter, 1989). In the first stage, when xanthan is exposed to disordering conditions, e.g., heating to a critical temperature (T_m) or upon exposure to low salinities (10^{-3}–10^{-4}M NaCl), lateral chains unfold, resulting in an extended, less compact and much more flexible double-helical structure (Muller & Lecourtier, 1988; Stokke et al., 1989). It has also been proposed that the double helix melts down from both ends to produce a dimerized expanded coil (Liu & Norisuye, 1988). At this step, the molecular weight (M_w) does not change but has a smaller persistence length and lower viscosity; upon cooling, the dimeric structure is reformed (Muller & Lecourtier, 1988). The second step is an intermolecular process and occurs under more severe conditions, i.e., salinities $\leq 10^{-5}$ M or exposure to a $T^{\circ} > T_m$ for large periods of time. Under such conditions, the M_w is roughly halved, indicating a complete dissociation of aggregates and double helices into single-stranded chains (Bezemer, Ubbink, de Kooker, Kuil, & Leyte, 1993; Muller & Lecourtier, 1988; Stokke et al., 1989).

Xanthan dispersions display, even at low polymer concentrations, unusually high viscosities and an important pseudoplastic behavior (Born et al., 2005), both of which are at the base of its attractive functional properties (i.e., suspending and stabilizing

* Corresponding author. Tel.: +1 418 656 2131x4970; fax: +1 418 656 3353.
E-mail address: Sylvie.Turgeon@fsaa.ulaval.ca (S.L. Turgeon).

0144-8617/$ – see front matter © 2012 Elsevier Ltd. All rights reserved.
http://dx.doi.org/10.1016/j.carbpol.2012.11.077

effect). The molecular origin of this behavior appears to be related to the molecule's structuration pattern in solution which includes hydrogen bridging between the lateral chains of adjacent molecules and molecular entanglements to form a loosely bound network (Born et al., 2005; Choppe, Puaud, Nicolai, & Benyahia, 2010; Norton et al., 1984). It has also been proposed that the extended conformation may promote mesomorphic organization (Lee & Brant, 2002; Milas, Rinaudo, Duplessix, Borsali, & Lindner, 1995; Schorsch, Garnier, & Doublier, 1996) or even the formation of a cholesteric phase (Rinaudo & Milas, 1982). This type of organization is typical of rigid or semi-rigid polymers, which, above a certain critical concentration, tend to spontaneously form ordered phases to reduce molecular excluded volume (Richardson & Ross-Murphy, 1987). Moreover, the unusual weak-gel and suspending properties of xanthan appear to be related to the formation of nematic phases in solution (Carnali, 1991). In xanthan gum, the transition to a cholesteric phase appears to be favored by lateral chain interactions via hydrogen bonding, and has been reported to occur at ~0.8% (w/w) (Carnali, 1991). On this basis, physical degradation is often viewed as having a negative impact on polymer functional properties (e.g. viscosity loss). However, several studies of polymer controlled degradation aiming to improve and/or to produce tailored functionalities for specific processes have been reported in food science (Corredig & Wicker, 2001; Evans & Marrs, 1997; Floury, Desrumaux, Axelos, & Legrand, 2002; Laneuville, Paquin, & Turgeon, 2000; Villay et al., 2012) as well as in pharmaceutics (Kojima, Tabata, Ikumoto, & Yanaki, 1984; Silvestri & Gabrielson, 1991).

The interest on characterizing the effect of microfluidization (a dynamic high-pressure treatment) on the physical properties of xanthan gum, was prompted by previous results on protein–xanthan gum associative interaction studies (Laneuville et al., 2000), where it was found that a microfluidization pretreatment on xanthan modified the functional properties of the resulting ingredient. Studies of dynamic high pressure treatments on polysaccharides report that degradation depends on several factors including the initial M_w and viscosity (Floury et al., 2002; Silvestri & Gabrielson, 1991; Villay et al., 2012), the applied pressure (Floury et al., 2002), the molecular structure (Villay et al., 2012), the solvent composition (Cencia-Rohan & Silvestri, 1993), and the pH (Chen et al., 2012). Mechanical stresses such as those encountered during microfluidization have been reported to disrupt aggregates (Corredig & Wicker, 2001; Lagoueyte & Paquin, 1998) or break covalent bonds of large molecules if a critical shear force (specific to each polymer-solvent system) is exceeded (Cencia-Rohan & Silvestri, 1993; Kojima et al., 1984; Silvestri & Gabrielson, 1991; Villay et al., 2012). A previous paper reported that microfluidization only disrupted xanthan aggregates (Lagoueyte & Paquin, 1998); in this paper questions regarding molecular integrity and rheological behavior are addressed, moreover flow birefringence was studied, which allowed obtaining new evidence for the highly associative structure of xanthan.

2. Materials and methods

Xanthan gum, Keltrol F (lot no. 9D2192K), was obtained from CP Kelco Co. San Diego, CA. Aqueous xanthan dispersions (1 wt%) were prepared at ionic strengths of 10^{-4} M or 0.1 M NaCl using a high shear Stephan mixer (300 rpm/25 min) equipped with a vacuum pump. Samples were diluted directly at the desired ionic strength to minimize conformational changes (Milas & Rinaudo, 1986; Muller & Lecourtier, 1988), which could increase variability among samples. Samples were kept at 4 °C overnight. Subsequently, xanthan dispersions were circulated 1, 4, or 12 passes through a microfluidizer (110Y Microfluidics Corporation, Newton, MA) at 75 MPa. Samples will be referred to as 1P, 4P or 12P hereafter. During microfluidization, the temperature was controlled by covering the reaction chamber and outlet piping with ice; resulting in an outlet temperature of 20–25 °C. Samples were treated at the dispersion pH which was 6.1 ± 0.1.

Microfluidized samples were divided in two sets; one set was dialyzed using Spectrapor*4 membranes (Spectrum, MWCO = 12,000–14,000) against Milli-Q water for 4 days (4 °C) and 3 water changes per day. At the end of this time, the presence of chloride ions was not detected by the $AgNO_3$ assay in the dializate water (Harris & Kratochvil, 1974). Dialyzed samples were freeze-dried, milled and kept at room temperature until further analysis. Dialyzation was carried out to be able to control the amount of salt in the samples in the subsequent analyses. The second set was kept in solution after treatment and stored at 4 °C, with 0.05% NaN_3 added as a preservative, this set was only utilized for rheological or rheooptical measurements. Blank samples, designated as samples treated 0 passes (0P), were also prepared following all the described steps (solubilization either in 10^{-4} M or 0.1 M NaCl, dialyzed and lyophilized) except for the microfluidization treatment. Tests were also made on dispersions of xanthan gum "as received" (without the dialysis, lyophilization or microfluidization steps); these samples were designated as "Keltrol", this was done to be able to track any aggregation that may occur during the solubilization and lyophilization processes.

2.1. Chemical analyses

Keltrol, 0P, and microfluidized xanthan samples were characterized chemically. Protein content was determined by measuring total nitrogen by combustion according to the Dumas principle (IDF standards 185:2002) using a LECO equipment (FP-528, Leco Corporation, St. Joseph, MI) and a conversion factor of 6.25. Total carbohydrate content was determined by the phenol–sulfuric acid method using D-glucose as standard. Reducing ends were assayed by the Nelson reagent method (Hodge & Hofreiter, 1962). The degrees of pyruvilation and acetylation were determined by H^1-RMN using a 200 MHz Varian XL spectrometer (Varian Associates, Palo Alto, CA). The substituents content was estimated by measuring the peak areas of the acetate (δ = 2.14 ppm) and pyruvate (δ = 1.44 ppm) using 5 mM of sodium acetate (δ = 1.89 ppm) as internal standard.

2.2. Physical analysis

For all tests, xanthan samples were dispersed 24 h prior to the analysis, left overnight at 4 °C, and then left to stand at room temperature for 1 h before measurements. Concentrations and solvents used are specified in each section.

2.2.1. High performance size-exclusion chromatography–multiangle laser light scattering (HPSEC–MALLS)

The average molecular weight of the xanthan samples was determined by HPSEC–MALLS. The HPSEC system consisted of a Waters 515 HPLC pump (Waters Chromatography S.A., Milford, USA), a 200 μL manual injecting loop and a Wyatt Optilab 903 refractometer (Wyatt Technology, Santa Barbara, USA). The MALLS apparatus was equipped with a Wyatt Dawn-DSP laser photometer (Wyatt Technology, Santa Barbara, USA), a K5 flow cell and a He–Ne laser operating at λ = 632.8 nm. The detection of scattering light was possible at 16 angles. The sensitivity level was set to X20. Prior to measurements, the Dawn apparatus was normalized using pullulan standard (P-50 Shodex, Japan). Three columns were used in line: TSK-guard column PWXL (6 mm × 40 mm), TSK-G6000 PW (7.5 mm × 300 mm) and a TSK-G4000 PW (7.8 mm × 300 mm) (Tosoh Bioscience, Montgomeryville, USA). Xanthan samples were

redispersed (1 mg/ml) in the mobile phase (0.1 M $NaNO_3$ – 0.05% NaN_3), and filtered through 5.0 and 1.2 μm Pall filters (Acrodisc syringe filters 32 mm with Supor® Membrane, Pall Newquay, Cornwall, UK, Pall corporation) prior injection. The flow rate was 0.5 mL/min and analyses were performed at room temperature. Obtained data was analyzed using the Astra software version 4.5 (Wyatt Technology Corp.), M_w were estimated using a $dn/dc = 0.145$ mL/g and a fourth-order Debye (Wyatt, 1993), the Debye model has been reported to be better suited to determine the M_w of xanthan gum (Born et al., 2005).

2.2.2. Intrinsic viscosity

The intrinsic viscosity was measured in the dilute regime in 0.01 M NaCl. Five different concentrations were tested: 0.01–0.25 g/L at intervals of 0.05 g/L. Eight measurements were taken for each sample using a rolling ball viscosimeter AMV200 (Paar Physica, Glen Allen, VA) with a capillary of 1.6 mm diameter and a ball 1.5 mm diameter (density: 7.85 g/cm^3). Measurements were taken at 25 °C at an inclination angle ø = 20. Intrinsic viscosities [η] were calculated by extrapolation of the reduced and inherent viscosities to infinite dilution using the Huggins' and Kraemers' equations (Bohdanecky & Kovař, 1982). The mean difference between these two values was of the order of 0.8%, which was considered very low, thus mean values are presented. The use of mean values of [η] has been discussed elsewhere (Bohdanecky & Kovař, 1982). The Huggins constant k_H was calculated to obtain a rough estimation of the samples' molecular aggregation degree (Sato, Norisuye, & Fujita, 1985).

2.2.3. Rheometry

Flow curves were obtained for xanthan samples re-dispersed at 0.5 wt% in 0.05 M NaCl. Tests were also conducted on samples that were kept in cold storage (1 wt% + NaN_3) 48 h or 2 months after microfluidization. Measurements were performed at 25 °C with a shear-rate controlled rheometer (ARES-100FRT, TA-Instrument, New Castle, DE) equipped with a couette-type sensor. The inner and outer cylinder radiuses were 32 and 34 mm respectively; the length of the inner cylinder was 33.3 mm. The shear-rate range explored was from 0.1 s^{-1} up to 2520 s^{-1}. To compare the flow curves, data was fitted using the Cross model (Cross, 1969):

$$\eta = \frac{\eta_0}{1 + (\tau\dot{\gamma})^m} \quad (1)$$

where η is the viscosity at a given shear rate $\dot{\gamma}$; η_0 is the viscosity at low shear rate; τ is a relaxation time so that $\dot{\gamma}_c = 1/\tau$ (s^{-1}), which is a characteristic shear rate for the onset of the shear thinning regime; and m is the slope of the high shear-rate portion of the curve. Error bars will be presented only in the first point of each curve for clarity.

2.2.4. Flow birefringence

Flow birefringence was measured on xanthan gum samples re-dispersed at 0.25 wt% in 10^{-4} M or 0.1 M NaCl. Samples at 1 wt% kept in cold storage after microfluidization were also tested. Measurements were performed at room temperature with a shear stress controlled rheometer (SR-5000, Rheometric Scientific, Piscataway, NJ) equipped with an Optical Analysis Module (OAM) and a quartz parallel plate geometry (32 mm diameter). The laser emitting at a wavelength λ of 632.8 nm passed through the sample (1 mm gap) at normal incidence. Two types of tests were carried out. A rate ramp test where shear rate was increased from 0 to 500 s^{-1} in 500 s. The second test was a step rate test, where sequential steady shear rates were applied as follows: 0, 1, 10, 100, 500 and 0 s^{-1}, each step lasted 100 s. Flow induced birefringence (Δn) and extinction angle (χ), characterizing the average orientation of the molecules in the flow direction, were measured and used to determine the start-up and steady state birefringence. These tests allowed evaluating the molecular organization and the behavior of xanthan molecules and/or aggregates during flow. For clarity, no error bars will be presented in the figures. Triplicate assays showed a standard deviation of ±0.3 to 0.5%, depending on the concentration.

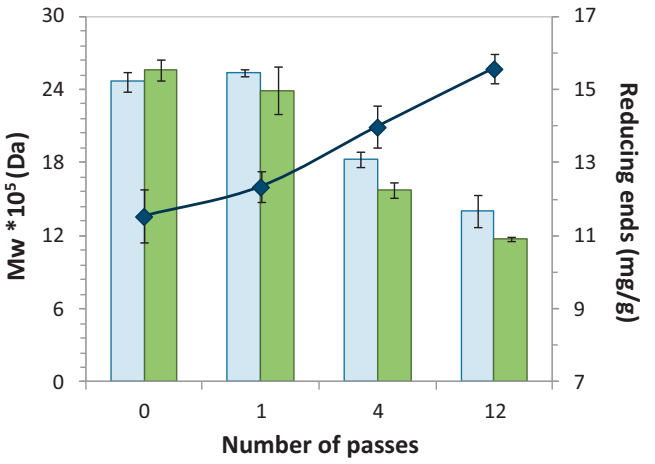

Fig. 1. M_w of microfluidized xanthan in 10^{-4}M (□)or in 0.1 M NaCl (■) measured by HPSEC–MALLS. Secondary axis: reducing ends (♦).

Typical values for the overlap concentration, c^*, of xanthan dispersions are in the order of $[\eta]^{-1}$ and ranges from 0.02 to 0.1 wt%, whereas the onset of the concentrated regime, c^{**}, approximates $8[\eta]-1$ and is usually found around 0.65 wt% (Lim, 1984; Lo et al., 2009; Meyer, Fuller, Clark, & Kulicke, 1993; Rochefort, 1987). Therefore, tests carried at 0.25 or 1.0 wt% were within the theoretical semidilute or concentrated regimes.

2.3. Statistical analysis

Data was compared using the t-test (LSD), with $\alpha = 0.05\%$ confidence using the SAS/STAT Language (SAS Institute Inc., Cary, NC).

3. Results and discussion

3.1. Chemical characterization

Xanthan gum samples contained 96.36% total sugars and 3.60% protein (non dialyzable, thus accounted as cellular debris). The pyruvate content was 3.76 ± 0.08 mg/100 g, which corresponds to ~43.2% pyruvilation. This value approaches the typical value of 50% pyruvilation reported for Keltrol samples, corresponding to a xanthan repeating unit bearing one pyruvic acid ketal on every other terminal D-mannose unit (Holzwarth, 1976). The level of acetylation was 85 ± 3 mg/100 g which corresponds to ~98.3% acetylation. The acetate and pyruvate content remained constant throughout the microfluidization process, indicating that lateral chains were not affected by microfluidization.

On the other hand, the relative amount of reducing ends (Fig. 1, secondary axis) showed a slight but significant increase from ~11 mg/g for 0P samples to ~15.6 mg/g for xanthan treated 12P ($p < 0.01$). No significant increase in reducing ends was found in samples treated 1P compared to the 0P samples, showing that after the first pass through the microfluidizer, the molecules remained essentially intact. Overall, a tendency towards higher degradation was noted for samples in 0.1 M compared to those in 10^{-4} M; however, this difference was not statistically significant, therefore mean values are presented.

Table 1
Physical parameters measured for xanthan microfluidized in 10^{-4} M or 0.1 M NaCl.

	Intrinsic viscosity parameters		HPSEC–MALLS	Viscosity curve fitting			Birefringence parameters[d]		
Keltrol	$[\eta]$ (ml/g)	k_H	Rg (nm)	η (Pa s)	$\dot{\gamma}_c(s^{-1})$	m	χ_{ini}	$\dot{\gamma}_{sat}(s^{-1})$	$\Delta\eta_{final}$
10^{-4} M[a]	2530b	0.69a	149.0a	–	–	–	–	–	–
0	2773a	0.78a	148.0a	26.7[b],a	0.017a	0.18a	31.3b	12b	75.5b
1	1877c	0.54bc	149.8a	2.6[b],b	0.056a	0.41b	25.7a	9a	80.9a
4	1434d	0.53bc	143.8a	0.44[c]	0.163b	0.56c	40.0d	35e	70.3c
12	1075f	0.45d	133.6b	0.07[e]	16.55d	0.55c	44.9e	78h	51.8d
0.1 M[a]									
0	2665a	0.74a	150.9a	30.1[b],a	0.017a	0.18a	28.2a	18c	34.6f
1	1763c	0.56b	146.3a	2.4[b],b	0.55a	0.41b	37.9c	13b	44.3e
4	1255e	0.46cd	136.7b	0.14d	2.60c	0.59c	35.5c	40f	37.9f
12	888[g]	0.47cd	123.6c	0.05f	16.53d	0.60c	37.1c	115j	23.7g

[a] Ionic strength during microfluidization. Ionic strength during physical analyses is described in Section 2.
[b] η_o was not measurable under the studied conditions for 0P and 1P, the presented value is the viscosity at 0.1 s^{-1}.
[c] In each column, values bearing the same letter are not statistically different at 0.05% confidence.
[d] Values from the rate ramp test on samples at 1 wt%.

3.2. Molecular weight and intrinsic viscosity

The M_w (Fig. 1) and intrinsic viscosities $[\eta]$ (Table 1) for the Keltrol and 0P samples are in the same order of magnitude than that found by several other authors working under similar experimental conditions and corresponds to a double stranded conformation (Chauveteau & Kohler, 1984; Holzwarth, 1976; Milas et al., 1996; Muller et al., 1986; Sato et al., 1984). Results show that after 1 pass there is no significant decrease in the M_w, however; the reduction in $[\eta]$ is substantial. After 4 passes, the M_w decreased to $\sim 17 \times 10^5$ Da (Fig. 1) and the $[\eta]$ approached previously reported values for sonicated single stranded xanthan samples $[\eta] = 1230$ ml/g (Milas et al., 1996), or for single xanthan chains in 10^{-5} M NaCl, $[\eta] = 1500$ ml/g (Muller et al., 1986). However, this reduction may be related to a decrease in M_w rather than in a separation of the double stranded structure since this test was carried out at high ionic strengths and other studies have shown that xanthan can maintain a double stranded conformation till very advances stages of hydrolysis (Christensen, Smidsroed, Elgsaeter, & Stokke, 1993). After 12 passes, the degradation in the main chain is evident by an important decrease in M_w and a continual increase in reducing ends (Fig. 1). However, a high molecular mass ($>10^5$) was retained in all samples, indicating only mild degradation. Polydispersity (M_w/M_n) increased slightly from 1.07 ± 0.01 to 1.23 ± 0.09, for 0P and 12P respectively when treated in 10^{-4} M NaCl. In 0.1 M the effect was not statistically significant and $M_w/M_n \sim 1.17 \pm 0.04$. The obtained radius of gyration (Rg) for the 0P and 1P samples are in agreement with previously reported values for native xanthan in a double helix conformation of 120–170 nm (Capron, Brigand, & Muller, 1997; Milas et al., 1996). Rg decreased slightly for 4P and 12P, again indicating a mild degradation (Table 1).

The Huggins constant k_H was obtained from the fitting of the intrinsic viscosity data, although this parameter alone does not allow concluding on the aggregation level in a sample, it can give a rough estimation of polymer–polymer interaction. k_H can take values between 0.3 (in good solvents) and 0.5, while values as high as 0.8 are considered to be normal, values higher than unity indicate important aggregation (Sato et al., 1985). Keltrol and 0P samples presented k_H values between 0.7 and 0.8 (Table 1), indicating some aggregation (Bohdanecky & Kovař, 1982). The slightly higher $[\eta]$ and k_H values for 0P samples compared to the Keltrol sample (Table 1), points to some aggregation induced by the solubilization/dialization steps, as is commonly known to occur in xanthan during these processes. The k_H obtained for microfluidized xanthan samples was lower and approached that of xanthan measured above 50 °C ($k_H = 0.40$–0.45) (Muller & Lecourtier, 1988), indicating fewer molecular associations.

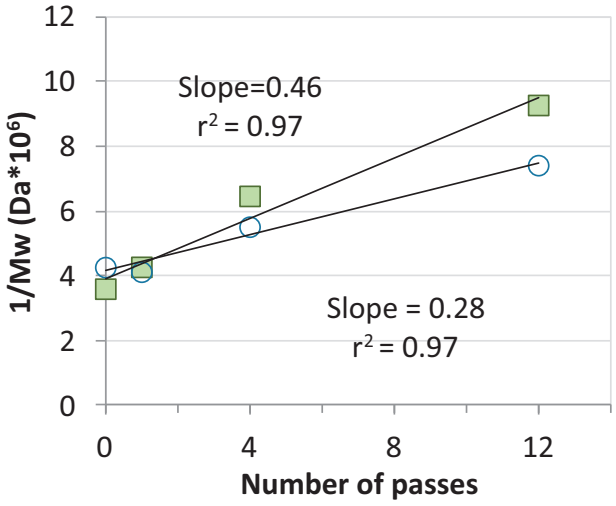

Fig. 2. Apparent degradation rate constants for xanthan microfluidized in 10^{-4}M (○) or in 0.1 M NaCl (■) at 75 MPa (error bars are smaller than data points).

Interestingly, the results revealed that the degradation was more pronounced for samples treated in 0.1 M NaCl (Fig. 1 and Table 1). Previous studies on acidic, oxidative or enzymatic degradation of xanthan gum (Hjerde, Kristiansen, Stokke, Smidsr, & Christensen, 1994; Milas, Rinaudo, & Tinland, 1986) have shown that xanthan is more stable in the ordered conformation (high ionic strength) due to the alignment of the side chains along the backbone, which shields the glycosidic linkages (Hjerde et al., 1994). Moreover, it has been reported that xanthan is more stable against degradation, compared to other biopolymers, only when in the ordered state (Hjerde et al., 1994). During microfluidization, the induced degradation obeys random scission kinetics (Cencia-Rohan & Silvestri, 1993; Silvestri & Gabrielson, 1991) and the apparent mechanical degradation rate constant (k_d) can be approximated from the slope of a plot of $1/M_w$ vs. the severity of the treatment (in this case, the number of passes). Such plot is presented in Fig. 2, which shows that the data for microfluidized samples are well described by a single constant decay, confirming that the degradation rate in 0.1 M NaCl is higher than in 10^{-4} M NaCl.

At high ionic strengths, xanthan dispersions were more viscous since molecules in the ordered conformation presented larger hydrodynamic sizes. The reported persistence length, of the ordered conformation is of 120–150 nm (Muller et al., 1986; Muller & Lecourtier, 1988; Sato et al., 1984) and indicates a much more stiff conformation compared to the persistence length of 60–70 nm

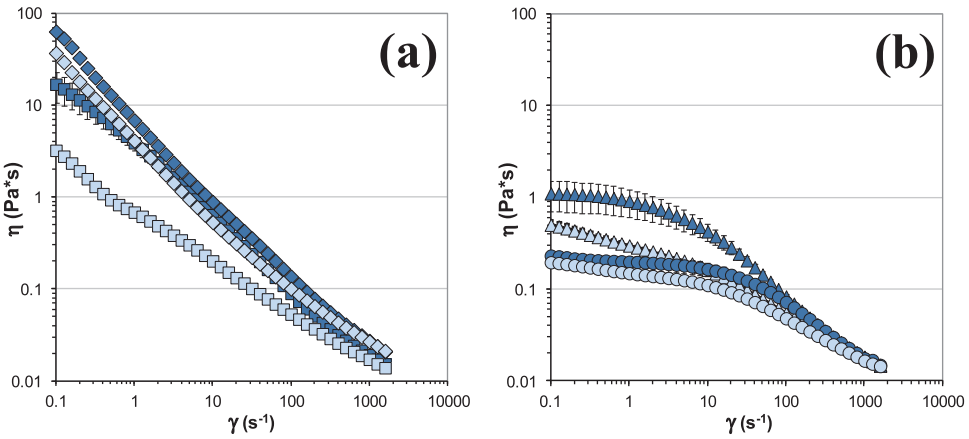

Fig. 3. Flow curves for samples microfluidized in 10^{-4}M NaCl (1 wt%), 2 days after treatment (open symbols) or two months after treatment (filled symbols). (a) 0 passes (◊,♦) and 1 pass (□,■); (b) 4 passes (△,▲) and 12 passes (○,●).

for the disordered conformation (Stokke et al., 1989). We propose that xanthan in its ordered state presents a larger exposed surface which in combination with a stiffer conformation experience stronger effective stresses than flexible chains when subjected to the high shear and cavitation forces present in the microfluidization chamber. Since samples at high ionic strength were more viscous and since higher viscosities results in lower Reynolds numbers (Floury et al., 2002), our results point to the important effect of shear stresses during mechanical degradation. Accordingly, another study on degradation by dynamic high pressures on acacia gum, CMC, alginate and guar gum (Villay et al., 2012), found that the sensitivity of polysaccharides strongly depend on their structure, with stiff polymers undergoing depolymerization, while flexible branched polysaccharides being nearly unaffected under the same conditions.

3.3. Flow behavior and viscosity recovery

3.3.1. Samples analyzed after cold storage in solution

Fig. 3 presents the viscosity profiles of xanthan samples (1 wt%) measured 2 days (open symbols) or 2 months (filled symbols) after microfluidization in 10^{-4} M NaCl and cold storage. It can be seen that after 2 months of storage, the viscosity of microfluidized samples increased, showing a time-dependent aggregation phenomenon and viscosity recovery.

Note that 0P samples in 10^{-4} M NaCl also showed a slight increase in its viscosity. This phenomenon has been previously reported in literature by several authors (Bezemer et al., 1993; Holzwarth, 1976; Rochefort, 1987) who observed a long term equilibration process of xanthan gum in deionized water and related to its aggregation tendency. Inter-chain association is a process that includes more than just molecular entanglements; there are specific interactions, principally hydrogen bonding and other forms of non covalent interaction (such as ionic interactions) (Choppe et al., 2010; Lo et al., 2009) controlled, in part, by environmental ionic strength and the levels of acetylation and pyruvilation of the sample (Frangou, Morris, Rees, Richardson, & Ross-Murphy, 1982). It is known that hydrogen bonding plays a major role in stabilizing xanthan aggregates since they do not form in the presence of urea, a known hydrogen-bond breaker (Lo et al., 2009; Southwick, Lee, Jamieson, & Blackwell, 1980). In our samples, hydrogen bonding may have been further favored by the low temperatures (4 °C) during storage.

The flow curves presented in Fig. 3a for samples 0P and 1P after 2 months of storage (filled symbols) resemble previously reported flow profiles of xanthan dissolved at different molar concentrations of urea. Increasing the levels of urea caused the disruption of aggregates, which translated into a decrease in the low-shear viscosity; and flow curves converging to a common high shear limit (Frangou et al., 1982). Another related study reports that a sample free of microgels (obtained by filtration) also presented a lower η_o region and a common high shear limit when compared to non-filtered samples (Chauveteau & Kohler, 1984). In this study, xanthan samples treated 1 pass in 10^{-4}M NaCl presented a remarkable viscosity recovery and the final viscosity profiles were very close to that of the 0P samples, except in the low shear rate region (<0.5 s^{-1}) (Fig. 3a), hence it can be concluded that 1P samples are predominantly free of microgels or aggregated structures, and as such can be considered to be xanthan solutions. From the results is also possible to see that large aggregates or microgels do not reform.

The extent of viscosity recovery in 1P samples is so important that ascribing it only to molecular entanglement and random aggregation appears highly unlikely. To explain these results, we hypothesize that viscosity recovery may be related to the restoration of double stranded structures disrupted during microfluidization. However, since no direct measurement were made on samples immediately after they left the microfluidization chamber, further investigation would be needed to confirm this proposition. Other authors have found that xanthan molecules do not always reform a perfectly paired double helix, instead single chain portions tend to randomly aggregate and may form multi-stranded structures and dimeric helices with a certain degree of mismatch, as observed by electron microcopy (Stokke et al., 1989). Such structures have a more extended conformation, larger hydrodynamic volume (more excluded-volume effect) and thus yield higher viscosities (Liu & Norisuye, 1988; Milas & Rinaudo, 1986).

For samples treated 4 passes, the recovery was less important, and the final viscosity remained very low. After 12 passes, viscosity recovery was almost negligible (Fig. 3b). The lack of viscosity recovery for the more degraded samples appear to be related to lower M_w and the inability of smaller molecules to form enough junction points to maintain the weak network xanthan usually forms. This is supported by the decrease in pseudoplastic behavior in 4P and 12P samples (Fig. 3a). In 0.1 M NaCl, no changes in the viscosity were observed after cold storage (results not shown). It is possible that there was some recovery but it occurred in a small window of time (<48 h) after microfluidization, such rapid re-aggregation would be favored by the screening of electrostatic repulsion from the

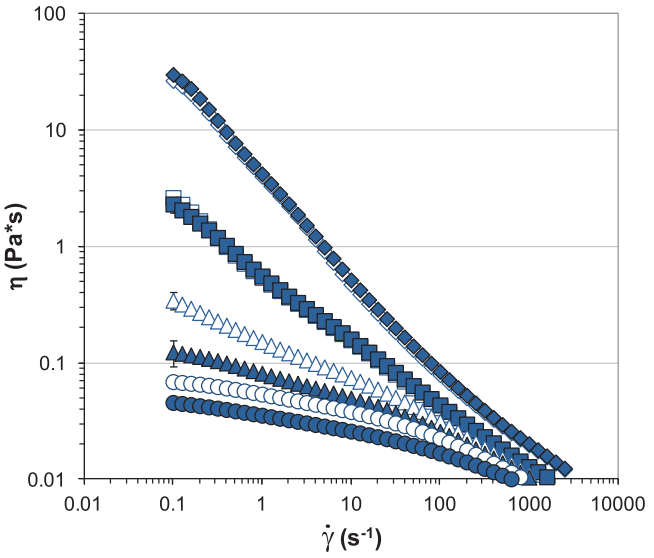

Fig. 4. Flow curves for xanthan microfluidized in 10^{-4}M NaCl (open symbols) or 0.1 M NaCl (filled symbols). 0 passes (◇,♦), 1 pass (□,■), 4 passes (△,▲), and 12 passes (○,●). Samples re-dispersed at 0.5 wt% in 0.05 M NaCl.

lateral chains due to the high ionic strength in the system (Rochefort, 1987).

3.3.2. Samples analyzed after dialyzation/lyophilization

To better compare samples, dialyzed and lyophilized samples were re-dispersed in the same solvent. Fig. 4 shows the apparent viscosity (η) with respect to the shear rate ($\dot{\gamma}$) for all samples re-dissolved at 0.5 wt% in 0.05 M NaCl. The Cross model fitting parameters are summarized in Table 1. The r^2 values of the fittings were ≥0.96 in all cases. Under the studied conditions, η_o for 0P and 1P samples could not be measured, therefore for these 2 samples, Table 1 presents the value of η measured at 0.1 s^{-1}.

In general, the number of passes through the microfluidizer had an influence on η, τ, and m. 0P samples presented higher viscosities over the whole range of $\dot{\gamma}$, and presented a power law region from the lowest studied rates of shear (0.1 s^{-1}) (Fig. 4). Samples treated 1P in either 10^{-4} M or 0.1 M NaCl presented a similar viscosity profile lower than 0P samples. Samples treated 4P converged to some extent to a common high-shear limit with 1P samples, whereas the more degraded samples (12 passes) presented overall lower viscosities. However, for 4P or 12P samples, viscosity loss was more pronounced in samples treated in 0.1 M NaCl (Fig. 4). The high-pressure reduced the pseudoplastic behavior and lowered η to ~0.20–0.35% of its initial value, depending on the severity of the treatment and the solvent in which the sample was treated (Table 1).

Since the viscosity at low rates of shear is a function of the volumic mass of a molecule, the reduction in η and in the shear-thinning behavior (indicated by the broadening of the curves and the decrease in the parameter τ) can be correlated to lower M_w and also to lower aggregate content. However, the important reduction in [η] (Table 1) may have also been enhanced by the increased polydispersity in the system. The coefficient m is related to the polydispersity of the system. Low polydispersity generates a large slope for the flow curve (Cross, 1969). From data in Table 1, it is possible to see that microfluidization broadens the curves and render them more flat. The decrease in m and pseudoplasticity is highly related to M_w decrease, these results indicate that degraded samples present lower suspending ability. The decrease in pseudoplastic behavior may have also been promoted by the increased polydispersity, as measured by MALLS, since small particles fit between larger ones minimizing particle interactions resulting in a decrease of the pseudoplastic behavior (Luckham & Ukeje, 1999). Increased polydispersity was also observed on pectins after valve homogenization (Corredig & Wicker, 2001).

Additionally, Fig. 4 shows that the transition from Newtonian to pseudoplastic behavior (power law region) which occurs at the critical shear rate $\gamma_c = 1/\tau$, shifted to higher shear rates with increasing the number of passes; which can be related to lower M_w (Milas et al., 1986).

It has been reported that the rate of polymer degradation induced by microfluidization increases by increasing the viscosity of the initial solution and the radius of gyration of the polymer (Cencia-Rohan & Silvestri, 1993; Kojima et al., 1984; Villay et al., 2012). Accordingly, all of the mechanical-induced degradation studies cited herein report that the decrease in the measured physical parameters is not linear with treatment severity, the decrease being more important for the first treatments then tending to approach a constant value. This effect is markedly evident in the measured viscosity, for samples treated 1 pass, which presented a strong loss in [η] and η_o (Table 1). Since the M_w is not affected after 1P, the reduction in [η] and η_o appear to be related to the disruption of aggregates, at more severe treatments e.g. 4P, the backbone of the molecule is attacked evidenced by the increase in reducing ends.

3.4. Flow birefringence: rate ramp test

The birefringence (Δn) and extinction angle (χ) versus shear rate ($\dot{\gamma}$) for samples in 10^{-4} M NaCl at 1 wt% are presented in Fig. 5. The data for the 0P sample in 0.1 M NaCl at 1 wt% is also presented for comparison. The Δn was positive and increased with increasing shear rate (Fig. 5a), whereas χ decreased due to the progressive orientation of the molecules in the flow direction (0°) (Fig. 5b). Theory predicts the saturation of Δn and χ at high enough rates of shear (Chassapis, Balouktsis, & Karapantsios, 2002) indicating the alignment of molecules in the flow direction (Decruppe & Ponton, 2003). The resulting smooth curves of Δn and χ (Fig. 5) are a typical response of long rigid molecules (Decruppe & Ponton, 2003).

At rest, 0P samples presented a $\chi \sim 30°$ (Table 1), indicating some molecular alignment; this behavior is typical of xanthan gum and other long rigid or semi-rigid polymers above a certain concentration (Lee & Brant, 2002; Lo et al., 2009; Rinaudo & Milas, 1982; Schorsch et al., 1996). A completely random molecular orientation would give $\chi \sim 45°$.

Under quiescent conditions, 0P samples showed higher birefringence than treated 1P samples in 10^{-4} M NaCl, and continued to do so at low enough rates of shear ($\dot{\gamma} < 7\ s^{-1}$) (Fig. 5c). This result was surprising since the main difference between 0P and 1P samples was the aggregate content, such result suggests that the higher birefringence for 0P samples under quiescent conditions is promoted by the aggregate content, this is contradictory to the notion that aggregates hinder the formation of ordered phases (Meyer et al., 1993).

Interestingly, at sufficiently high shear rates ($\dot{\gamma} < 7\ s^{-1}$), xanthan microfluidized 1 pass became more birefringent than untreated samples (Fig. 5a and c). Moreover, molecules in samples treated 1 pass oriented more rapidly, lower $\dot{\gamma}_{sat}$, compared to 0P samples (at both studied high ionic strengths) and resulted in higher final birefringences ($\Delta\eta_{final}$) (Table 1). These results supports the flow and viscosity recovery results (Section 3.3) showing again that xanthan treated 1P is a sample free of aggregates or microgels and that aggregates do hinder molecular orientation.

Under quiescent conditions, the molecular orientation angle (χ_{ini}) was higher for the most degraded samples (Table 1), indicating a higher randomness of the molecular orientation, even at the high concentration of 1 wt%. This can be explained by smaller

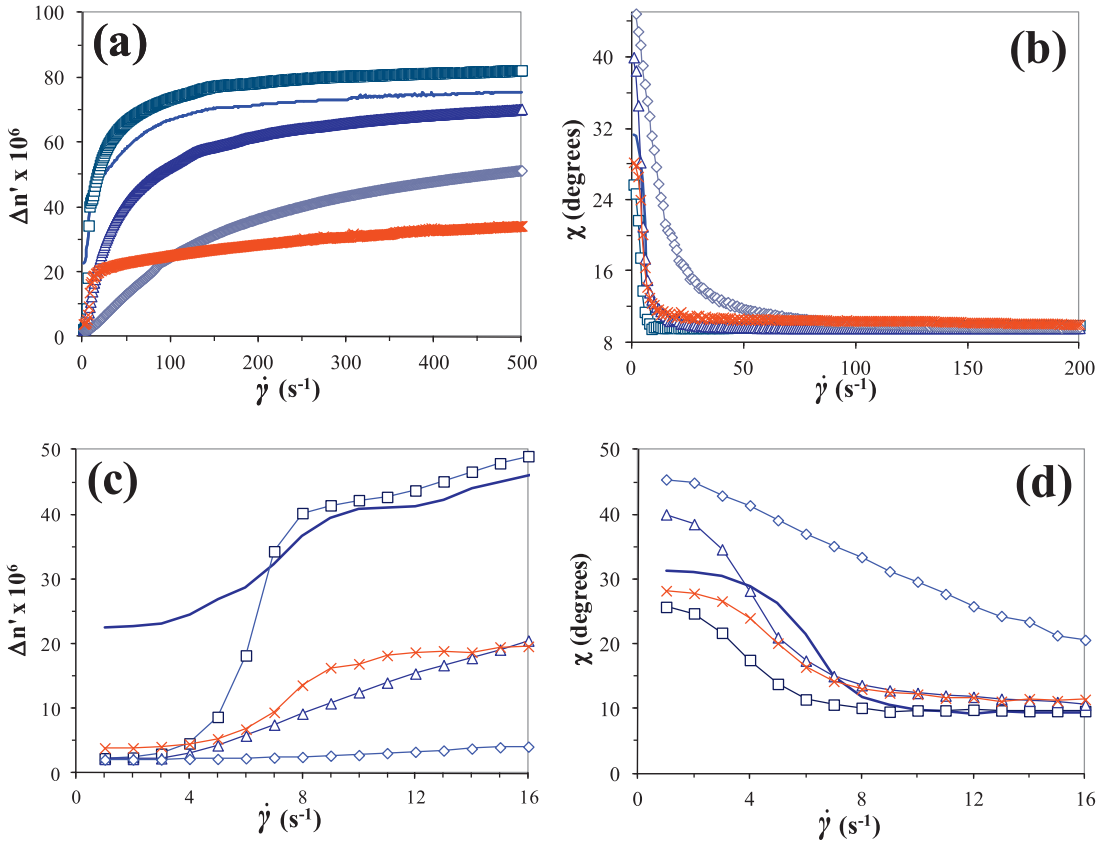

Fig. 5. Rate ramp test. (a) Flow birefringence (Δn) and (b) orientation angle (χ) for xanthan samples in 10^{-4}M NaCl (1 wt%), 0 passes (—), 1 pass (□), 4 passes (△), 12 passes (◊), and 0P in 0.1 M NaCl (1 wt%) (×). (c) and (d) are close-ups of the low shear regions for figures (a) and (b) respectively.

molecules exhibiting less orientational anisotropy since they are easily perturbed by Brownian motion. Moreover, when polydispersity increases (Table 1), molecular orientation can be further hindered by smaller particles infiltrating between larger ones, thus amplifying the effect (Johnson & Fuller, 1988).

Upon shear inception, molecular orientation occurred promptly for 0P, 1P and 4P samples, whereas it occurred more gradually for 12P samples (Fig. 5d), indicating that the more degraded samples required higher rates of shear to become aligned and attain saturation (Chassapis et al., 2002; Chow, Fuller, Wallace, & Madri, 1985; Lee & Brant, 2002). The molecular orientation for the less degraded samples may have been further favored due to segment-segment interaction which hinders Brownian motion, the latter tending to randomize molecular orientation (Meyer et al., 1993). The smaller final birefringence ($\Delta\eta_{final}$), the gradual molecular orientation and the higher rates of shear required to achieve saturation ($\dot{\gamma}_{sat}$) (Fig. 5a and Table 1) for 4P or 12P samples can be related to lower M_w (Chassapis et al., 2002; Chow et al., 1985). The same general behavior was observed when samples were tested at lower concentrations (0.25 wt%), with 1P samples presenting a higher birefringence at $\dot{\gamma} > 350\,s^{-1}$, and saturation being achieved at very high rates of shear, regardless of ionic strength (not shown).

The same test was carried out with samples re-dispersed in 0.1 M NaCl, similar trends were observed, however, the measured birefringences were much lower than in 10^{-4} M NaCl due to the increased rigidity of the chains at high salt contents (Meyer et al., 1993). When samples are redispersed in 10^{-4} M NaCl, xanthan molecules (in the disordered or extended conformation) could be stretched and aligned more easily by flow forces resulting in a net increase in molecular orientation and higher birefringence.

Birefringence measurements coupled with the observed viscosity recovery clearly show the tendency of xanthan molecules to reorganize and self-associate at low ionic strengths. Besides the ability of xanthan to form mesomorphic phases (Lee & Brant, 2002; Milas et al., 1995; Schorsch et al., 1996), light scattering studies have shown that xanthan structure formation presents a specific correlation length (Milas et al., 1995) and specific attractive interactions are involved (Choppe et al., 2010). Although a mechanism cannot be drawn, our results support the existence of such a structuration pattern in xanthan dispersions at low ionic strength. This structuration could explain the higher Δn found in 0P samples and at low rates of shear ($<\sim 10\,s^{-1}$) (Fig. 5c) compared to 1P samples in low ionic strengths.

3.5. Flow birefringence: step rate test

Fig. 6 presents the birefringence and orientation angle obtained in the step rate tests for samples re-dispersed at 0.25 wt% in 10^{-4} M NaCl. It can be observed that the birefringence reaches a steady state value almost immediately after flow inception at $t = 50$ s (or at flow rate increments); and rapidly relaxes to the initial value when flow is stopped at $t = 550$ s. This type of behavior is typical of semidilute solutions of rigid rods (Gatzonis, Siddiquee, & van Egmond, 1997). The transient response of Δn and χ depended on the degree of degradation, with the shear rate needed to induce a detectable Δn (or molecular orientation) increasing as the M_w decreased. For 0P samples, Δn appeared from the lowest applied shear rate ($\dot{\gamma} = 1\,s^{-1}$), with χ showing that the molecules were almost fully oriented (Fig. 6a and b). For samples treated 12 passes, a slight molecular orientation occurred at ($\dot{\gamma} = 50\,s^{-1}$) (Fig. 6b), however, this was not high enough to produce birefringence (Fig. 6a). For these samples, birefringence faintly appeared at ($\dot{\gamma} = 100\,s^{-1}$) with an orientation angle of a mere ~33°. The maximum Δn measured for samples treated 12P at $500\,s^{-1}$, was 70% lower than that

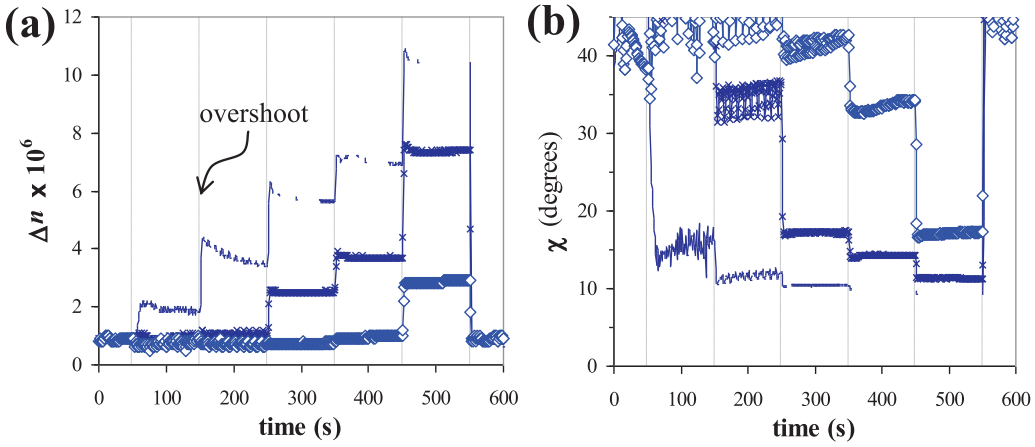

Fig. 6. Transient birefringence. Step rate tests, flow birefringence (Δn) and orientation angle (χ) for xanthan samples re-dispersed at 0.25 wt% in 10^{-4}M NaCl. 0 passes (—), 1 pass (x) or 12 passes (◊). Flow inception begins at $t = 50$ s, shear rate steps were of 0, 1, 10, 50, 100, 500 and 0 s^{-1}.

for 0P samples. The lower orientation angle for 4P and 12P samples may have been further induced by the increased polydispersity of the system (Johnson & Fuller, 1988) (Table 1).

In the step rate test at a concentration of 0.25%, the Δn induced by 0P samples was always higher than that for the 1P samples, contrary to the ramp rate test at 0.25 wt%, where 1P samples had higher birefringence than 0P samples at sufficiently high shear rates. However, at 1 wt% 1P samples presented a higher Δn at $\dot{\gamma} \geq 10\,s^{-1}$ (not shown). This difference may be related firstly to the concentration but also to the way in which the shear is applied (abrupt increases in this test compared to a gradual increase in the rate ramp test).

Birefringence overshoots can be seen in Fig. 6a for the 0P sample. The percentage of overshoots was measured as $(\Delta n_{max} - \Delta n_{steady})/\Delta n_{steady} \times 100\%$ (Chai, Creissel, & Randrianantoandro, 1999). The 0P sample had a ~26% overshoot at $\dot{\gamma} = 10\,s^{-1}$, and a smaller one (≤10%) at $\dot{\gamma} = 50\,s^{-1}$. The same tendency was found at higher ionic strengths, although smaller overshoots were measured (~13% at $\dot{\gamma} = 10\,s^{-1}$). Overshoots diminished greatly in 1P samples and occurred at much higher shear rates (~3% at $\dot{\gamma} = 500\,s^{-1}$). For the most degraded samples, no overshoots could be detected. At a concentration of 1 wt%, overshoots of 34% and 28% were observed at $\dot{\gamma} = 1\,s^{-1}$ in 10^{-4} M NaCl for 0P and 1P samples respectively (not shown).

The occurrence of birefringence overshoots is widely reported in literature for synthetic polymers (Chai et al., 1999; Gatzonis et al., 1997) and biopolymers (Chow et al., 1985; Meyer et al., 1993). Several explanations have been proposed for their presence depending essentially on the concentration regime. At low concentrations, overshoots have been considered to be caused by molecular stretching (Chai et al., 1999; Gatzonis et al., 1997). Whereas at higher concentrations, overshoots indicate a rapid breakdown of large structures present prior to flow inception (Lim, 1984). Overshoots may also reflect a rapid increase and decrease in the orientation of large aggregates (Meyer et al., 1993). Additionally, overshoots appear to be more susceptible to occur at higher molecular weights, since large molecules stretch more easily (Gatzonis et al., 1997). In this sense, the loss of overshoots for the most degraded samples supports a lower M_w. However, since overshoots were also greatly diminished in samples treated 1P, which presents essentially the same M_w as 0P samples (Fig. 1), it can be concluded that overshoots significantly depend on aggregate content (aggregate breakdown and/or stretching). It has been suggested that overshoots might be caused by the stretching of wormlike multi-chain aggregates (Gatzonis et al., 1997). This would be consistent with the known tendency of xanthan to aggregate. The larger overshoots in 10^{-4} M NaCl also suggest that at low ionic strengths, xanthan aggregates are more loosely bound and stretch with greater ease in the flow direction than aggregates at higher ionic strengths. This is in agreement with previous rheological studies where it was found that xanthan aggregates at low ionic strengths can be disrupted more easily than their counterparts in salt aqueous dispersion (Lim, 1984).

3.6. Proposed mechanism of xanthan degradation by microfluidization

Based on the analysis of our results we propose the following mechanism for the degradation of xanthan by microfluidization: In the first pass through the microfluidizer, the high shear forces disrupt the aggregates or microgels, resulting in xanthan solution (i.e., absence of aggregates). The disruption of large aggregates is supported by rheometry results that show that after 1 pass, viscosity cannot be recovered in the low shear rate region where microgels show their presence (Chauveteau & Kohler, 1984); the absence of aggregates is further confirmed by rheooptical measurements. If more passes are applied, the expanded molecules are not able to restructure fast enough and the mechanical forces can attack the backbone. We propose that this step may include the disruption of the xanthan double helix; this is supported by the important viscosity recovery for samples treated 1 pass. However, it is important to note that although viscosity recovery results point to this scenario, no measurements were carried out on samples immediately after microfluidization, thus the disruption of the double helical structure remains a hypothesis. After 12 passes, the degradation of the backbone is evident as determined by the continual increase in reducing ends and the important loss in M_w, $[\eta]$ and the loss of viscosity recovery ability. Mechanical-induced degradation cannot continue indefinitely since there is a critical M_w, particular to each polymer - solvent system, after which the device will no longer have an effect (Cencia-Rohan & Silvestri, 1993; Floury et al., 2002; Kojima et al., 1984). However, it appears that this critical M_w was not reached in this study.

Finally, samples treated in 0.1 M NaCl were more susceptible to degradation arguably because at high ionic strengths molecules rapidly regain a stiff conformation due to the alignment of the side chains with the backbone, thus presenting a larger hydrodynamic volume and overall larger exposed surface, which renders them more vulnerable to the stresses caused by the high shear, turbulence, and cavitation forces encountered during microfluidization.

4. Conclusion

The objective of this study was to evaluate the effect of microfluidization (1, 4 or 12 passes at 75 MPa) on the physical properties of xanthan gum. Microfluidization reduced the intrinsic viscosity, pseudoplastic behavior and flow birefringence of treated samples. At low treatment severity (1 pass through the device), aggregates were disrupted while molecular integrity was maintained. The presence of aggregates or microgels had an important effect in the flow behavior, flow-induced birefringence and molecular orientation. Specifically, it was found that aggregates show their presence by a higher viscosity in the low shear rate region while maintaining a common high shear region with samples free of aggregates. Additionally, samples free of aggregates presented higher birefringences (at high enough rates of shear) than samples containing aggregated structures. It was found that xanthan spontaneously rearranges over time, shown by the viscosity recovery and a detectable birefringence under quiescent conditions, indicating the formation of mesomorphic phases despite the presence of aggregates.

A mechanism for the microfluidization-induced degradation of xanthan was proposed which includes initially, the disruption of aggregates, possibly followed by a reversible disruption of the double stranded conformation. We hypothesize that for more severe treatments, double helices may have been separated into single helices, rendering the backbone susceptible to degradation upon further circulations through the device. However, a double stranded conformation reforms upon stopping the high pressure treatment. Finally, stiffer xanthan molecules (in the ordered conformation) experienced larger effective stresses since the degradation induced in samples in 0.1 M NaCl was higher than the degradation induced in 10^{-4} M NaCl.

Although microfluidization did cause degradation of the main chain for the more severe treatments, lateral chains remained intact and the resulting degradation did not reach the much higher degradation levels commonly found during chemical or oxidation-induced degradation. Thus, microfluidization appears as a new means to achieve a controlled and relatively mild degradation of xanthan gum without affecting its chemical composition, thus enlarging its potential applications, e.g. for the development of novel food ingredients (Laneuville et al., 2000).

Acknowledgments

The authors acknowledge the financial support from NSERC industrial chair and industrial partners Novalait Inc., Agropur and Parmalat, and Mrs. Anne-Françoise Allain for professional technical support.

References

Bezemer, L., Ubbink, J. B., de Kooker, J. A., Kuil, M. E., & Leyte, J. C. (1993). On the conformational transitions of native xanthan. *Macromolecules*, *26*(24), 6436–6446.

Bohdanecky, M., & Kovař, J. (1982). *Viscosity of polymer solutions*. New York: Elsevier Scientific Pub. Co.

Born, K., Langendorff, V., & Boulenguer, P. (2005). *Xanthan. Biopolymers Online*. http://dx.doi.org/10.1002/3527600035.bpol5011

Capron, I., Brigand, G., & Muller, G. (1997). About the native and renatured conformation of xanthan exopolysaccharide. *Polymer*, *38*(21), 5289–5295.

Carnali, J. O. (1991). A dispersed anisotropic phase as the origin of the weak-gel properties of aqueous xanthan gum. *Journal of Applied Polymer Science*, *43*, 929–941.

Cencia-Rohan, L., & Silvestri, S. (1993). Effect of solvent system on microfluidization-induced mechanical degradation. *International Journal of Pharmaceutics*, *95*(1-3), 23–28.

Chai, C. K., Creissel, J., & Randrianantoandro, H. (1999). Flow-induced birefringence of linear and long chain-branched metallocene polyethylene melts subject to steady start-up flow. *Polymer*, *40*(15), 4431–4436.

Chassapis, D., Balouktsis, A., & Karapantsios, T. D. (2002). Flow birefringence of temporary polymer networks. *European Polymer Journal*, *38*(6), 1071–1078.

Chauveteau, G., & Kohler, N. (1984). Influence of microgels in polysaccharide solutions on their flow behavior through porous media. *SPE Journal*, *24*(3), 361–368.

Chen, J., Liang, R.-H., Liu, W., Liu, C.-M., Li, T., & Tu, Z.-C. (2012). Degradation of high-methoxyl pectin by dynamic high pressure microfluidization and its mechanism. *Food Hydrocolloids*, *28*(1), 121–129.

Choppe, E., Puaud, F., Nicolai, T., & Benyahia, L. (2010). Rheology of xanthan solutions as a function of temperature, concentration and ionic strength. *Carbohydrate Polymers*, *82*(4), 1228–1235.

Chow, A. W., Fuller, G. G., Wallace, D. G., & Madri, J. A. (1985). Rheooptical response of rodlike chains subject to transient shear flow. 2. Two-color flow birefringence measurements on collagen protein. *Macromolecules*, *18*(4), 793–804.

Christensen, B. E., Smidsroed, O., Elgsaeter, A., & Stokke, B. T. (1993). Depolymerization of double-stranded xanthan by acid hydrolysis: characterization of partially degraded double strands and single-stranded oligomers released from the ordered structures. *Macromolecules*, *26*(22), 6111–6120.

Corredig, M., & Wicker, L. (2001). Changes in the molecular weight distribution of three commercial pectins after valve homogenization. *Food Hydrocolloids*, *15*(1), 17–23.

Cross, M. M. (1969). Polymer rheology: Influence of molecular weight and polydispersity. *Journal of Applied Polymer Science*, *13*(4), 765–774.

Decruppe, J. P., & Ponton, A. (2003). Flow birefringence, stress optical rule and rheology of four micellar solutions with the same low shear viscosity. *The European Physical Journal E: Soft Matter and Biological Physics*, *10*(3), 201–207.

Evans, M. T. A., & Marrs, W. M. (1997). Enhanced functionality for food hydrocolloids by molecular weight control: innovation and the regulatory maze. *European Food and Drink Review*, 65–68. Autumn.

Floury, J., Desrumaux, A., Axelos, M. A. V., & Legrand, J. (2002). Degradation of methylcellulose during ultra-high pressure homogenisation. *Food Hydrocolloids*, *16*(1), 47–53.

Frangou, S. A., Morris, E. R., Rees, D. A., Richardson, R. K., & Ross-Murphy, S. B. (1982). Molecular origin of xanthan solution rheology: Effect of urea on chain conformation and interactions. *Journal of Polymer Science: Polymer Letters Edition*, *20*(10), 531–538.

Gatzonis, Y., Siddiquee, S. K., & van Egmond, J. W. (1997). Rheo-optical investigation of wormlike polymers in solution. *Macromolecules*, *30*(23), 7253–7262.

Harris, W. E., & Kratochvil, B. (1974). *Chemical separations and measurements: background and procedures for modern analysis*. Philadelphia: Saunders.

Hjerde, T., Kristiansen, T. S., Stokke, B. T., Smidsr, O., & Christensen, B. E. (1994). Conformation dependent depolymerisation kinetics of polysaccharides studied by viscosity measurements. *Carbohydrate Polymers*, *24*(24), 265–275.

Hodge, J. E., & Hofreiter, B. T. (1962). Determination of reducing sugars and carbohydrates. In R. L. Whistler, J. N. BeMiller, & F. Shafizadeh (Eds.), *Methods in carbohydrate chemistry* (pp. 380–394). NY and London: Academic Press.

Holzwarth, G. (1976). Conformation of the extracellular polysaccharide of *Xanthomonas campestris*. *Biochemistry*, *15*(19), 4333–4339.

Jansson, P.-E., Kenne, L., & Lindberg, B. (1975). Structure of the extracellular polysaccharide from xanthomonas campestris. *Carbohydrate Research*, *45*(1), 275–282.

Johnson, S. J., & Fuller, G. G. (1988). The optical anisotropy of sheared hematite suspensions. *Journal of Colloid and Interface Science*, *124*(2), 441–451.

Kojima, T., Tabata, K., Ikumoto, T., & Yanaki, T. (1984). Depolymerization of schizophyllan by controlled hydrodynamic shear. *Agricultural and Biological Chemistry*, *48*(4), 915–921.

Lagoueyte, N., & Paquin, P. (1998). Effects of microfluidization on the functional properties of xanthan gum. *Food Hydrocolloids*, *12*(3), 365–371.

Laneuville, S. I., Paquin, P., & Turgeon, S. L. (2000). Effect of preparation conditions on the characteristics of whey protein–xanthan gum complexes. *Food Hydrocolloids*, *14*(4), 305–314.

Lee, H.-C., & Brant, D. A. (2002). Rheology of concentrated isotropic and anisotropic xanthan solutions. 1. A rodlike low molecular weight sample. *Macromolecules*, *35*(6), 2212–2222.

Lim, T. (1984). Rheology of self?associating concentrated xanthan solutions. *Journal of Rheology*, *28*(4), 367.

Liu, W., & Norisuye, T. (1988). Order–disorder conformation change of xanthan in 0.01 M aqueous sodium chloride: Dimensional behavior. *Biopolymers*, *27*(10), 1641–1654.

Lo, Y. M., Ziegler, R. C., Argin-Soysal, S., Hsu, C. H., & Wagner, N. J. (2009). Effects of intermolecular interactions and molecular orientation on the flux behavior of xanthan gum solutions during ultrafiltration. *Journal of Food Process Engineering*, *32*(5), 623–644.

Luckham, P. F., & Ukeje, M. A. (1999). Effect of particle size distribution on the rheology of dispersed systems. *Journal of Colloid and Interface Science*, *220*(2), 347–356.

Matsuda, Y., Biyajima, Y., & Sato, T. (2009). Thermal denaturation, renaturation, and aggregation of a double-helical polysaccharide xanthan in aqueous solution. *Polymer Journal*, *41*(7), 526–532.

Meyer, E. L., Fuller, G. G., Clark, R. C., & Kulicke, W. M. (1993). Investigation of xanthan gum solution behavior under shear flow using rheooptical techniques. *Macromolecules*, *26*(3), 504–511.

Milas, M., Reed, W. F., & Printz, S. (1996). Conformations and flexibility of native and re-natured xanthan in aqueous solutions. *International Journal of Biological Macromolecules*, *18*(3), 211–221.

Milas, M., & Rinaudo, M. (1986). Properties of xanthan gum in aqueous solutions: Role of the conformational transition. *Carbohydrate Research*, *158*, 191–204.

Milas, M., Rinaudo, M., Duplessix, R., Borsali, R., & Lindner, P. (1995). Small angle neutron scattering from polyelectrolyte solutions: from disordered to ordered xanthan chain conformation. *Macromolecules*, *28*(9), 3119–3124.

Milas, M., Rinaudo, M., & Tinland, B. (1986). Comparative depolymerization of xanthan gum by ultrasonic and enzymic treatments. Rheological and structural properties. *Carbohydrate Polymers*, *6*(2), 95–107.

Muller, G., Aurhourrache, M., Lecourtier, J., & Chauveteau, G. (1986). Salt dependence of the conformation of a single-stranded xanthan. *International Journal of Biological Macromolecules*, *8*(3), 167–172.

Muller, G., & Lecourtier, J. (1988). Temperature-induced extension and dissociation of native Xanthan. *Carbohydrate Polymers*, *9*, 213–225.

Norton, I. T., Goodall, D. M., Frangou, S. A., Morris, E. R., & Rees, D. A. (1984). Mechanism and dynamics of conformational ordering in xanthan polysaccharide. *Journal of Molecular Biology*, *175*(3), 371–394.

Pelletier, E., Viebke, C., Meadows, J., & Williams, P. A. (2001). A rheological study of the order–disorder conformational transition of xanthan gum. *Biopolymers*, *59*(5), 339–346.

Richardson, R. K., & Ross-Murphy, S. B. (1987). Non-Linear viscoelasticity of polysaccharide solutions. 2: xanthan polysaccharide solutions. *International Journal of Biological Macromolecules*, *9*, 257–264.

Rinaudo, M., & Milas, M. (1982). Xanthan properties in aqueous solution. *Carbohydrate Polymers*, *2*(4), 264–269.

Rochefort, W. (1987). Rheology of xanthan gum: salt, temperature, and strain effects in oscillatory and steady shear experiments. *Journal of Rheology*, *31*(4), 337.

Sato, T., Norisuye Fujita, H., & Fujita, H. (1985). Double-stranded helix of xanthan: dissociation behavior in mixtures of water and cadoxen. *Polymer Journal*, *17*(5), 729–735.

Sato, T., Norisuye, T., & Fujita, H. (1984). Double-stranded helix of xanthan: dimensional and hydrodynamic properties in 0.1 M aqueous sodium chloride. *Macromolecules*, *17*(12), 2696–2700.

Schorsch, C., Garnier, C., & Doublier, J.-L. (1996). Comportement rhéo-optique des solutions de xanthane et des mélanges xanthane/guar. *Les Cahiers de Rhéologie*, *15*(1), 375–380.

Silvestri, S., & Gabrielson, G. (1991). Degradation of tragacanth by high shear and turbulent forces during microfluidization. *International Journal of Pharmaceutics*, *73*(2), 163–169.

Southwick, J. G., Lee, H., Jamieson, A. M., & Blackwell, J. (1980). Self-association of xanthan in aqueous solvent-systems. *Carbohydrate Research*, *84*(2), 287–295.

Stokke, B. T., Smidsrød, O., & Elgsaeter, A. (1989). Electron microscopy of native xanthan and xanthan exposed to low ionic strength. *Biopolymers*, *28*(2), 617–637.

Sworn, G. (2009). Xanthan gum. In A. Imeson (Ed.), *Food stabilisers, thickeners and gelling agents*, ISBN 978-1-405-13267-1 (pp. 325–342). Wiley-Blackwell.

Villay, A., Lakkis de Filippis, F., Picton, L., Le Cerf, D., Vial, C., & Michaud, P. (2012). Comparison of polysaccharide degradations by dynamic high-pressure homogenization. *Food Hydrocolloids*, *27*(2), 278–286.

Wyatt, P. J. (1993). Light scattering and the absolute characterization of macromolecules. *Analytica Chimica Acta*, *272*(1), 1–40.